

Design of an Optimal Digital IIR Filter for Heart Rate Variability by Photoplethysmogram

Jeom Keun Kim¹, Jae Mok Ahn^{2,*}

*^{1,2} Professor, College of Software, Hallym University, 1 Hallymdaehak-gil,
Chuncheon-si, Gangwon-do, 24252 South Korea.*

**Corresponding author*

ABSTRACT

Heart rate variability (HRV) is a noninvasive indicator for evaluating the imbalance of the autonomic nervous system (ANS). Electrocardiogram (ECG) has been used more widely than photoplethysmogram (PPG) to detect the correct peak-to-peak time intervals between two successive R waves (RRI). Recently, PPG has been proposed as a surrogate of ECG in HRV analysis because ECG measurements confer discomfort and inconvenience. However, PPG is very sensitive to motion artefacts resulting in poor estimation of normal beat-to-beat intervals (NNI) in the PPG signal. Therefore, in this study, an optimal infinite impulse response (IIR) bandpass filter (IIR BPF) based on the digital Butterworth transfer function was proposed to improve the estimation of NNI based on the PPG data. Three time-domain and two nonlinear HRV parameters were calculated from the PPG datasets and were compared with those derived from the ECG datasets to evaluate the filter performance. The results show that there is no significant difference between RRI and NNI in the estimation of the relative errors of SDNN, RMSSD, SDDSD, SD1, and SD2 based on the PPG and ECG HRV datasets. The proposed digital IIR BPF enhanced the performance of the motion artefact algorithm for peak detection and provided a better HRV estimate.

Keywords: photoplethysmogram, heart rate variability, impulse response, autonomic nervous system

1. INTRODUCTION

Heart rate variability (HRV) is a physiological activity reflecting the cardiovascular control by the autonomic nervous system (ANS) [1-3]. ANS regulation of various functions includes heart rate, respiration, and the functions of all internal organs and is related to various diseases. Thus, HRV estimation technology reflecting the activity of ANS has been used in various health monitoring systems [4,5]. However, the accurate detection of heartbeat interval used in ANS evaluation is essential for successful and precise HRV analysis. HRV parameters are traditionally obtained by calculating the R wave peaks of the QRS complexes in ECG. Heartbeat interval of two successive R waves (RRI) in ECG is believed to provide more accurate RRI than estimation based on a finger-type PPG. However, the traditional ECG measurement has several concerns, including discomforts and inconveniences: (a) the attachment of at least two cutaneous electrodes is required; (b) the metal material of electrodes may cause skin irritations in some subjects; and (c) supervision is required to use ECG [6]. For these reasons, several studies attempted to evaluate HRV parameters based on PPG measurements, that are a simple, low-cost, and easy-to-use replacement of ECG [7-9]. In this paper, we demonstrate that HRV analysis can be used to derive the HRV data from a finger-type PPG without ECG. A heartbeat interval in milliseconds in the PPG signal is defined as a period between successive normal peak-to-peak intervals (NNI) as shown in Figure 1. Normally, a complete heart cycle starts at the beginning of foot and ends with the next foot. Variations in the peak amplitude and the starting point of the PPG foot cause problems in detection of an accurate NNI per heartbeat. Moreover, since the PPG signal reflects the cutaneous blood flow in the vessels from the heart to the fingertips, PPG is susceptible to motion artefacts and a poor signal-to-noise ratio due to even a slight body movement. The fingertip PPG signal is based on optical measurements obtained by irradiating the skin surface at a wavelength using a light emitting diode (LED) source and detecting the intensity of transmitted light using a photodiode opposite to the LED. The wavelength and distance between the light source and the photodiode determine the penetration depth of the light. Light with a wavelength from 500 to 1100 nm (from green to infrared) can be used in PPG. A green LED is suitable due to large variations in intensity modulated by pulsatile absorption of the blood; however, green LED has the disadvantage of high sensitivity to body movement [10]. An infrared LED is better for the measurement of deep-tissue blood flow but is sensitive to changes in the volumes of the peripheral vessels, leading to motion artefacts in the PPG measurements. A red LED light has moderate absorption by oxyhemoglobin and deoxyhemoglobin compared to green and infrared LEDs [11-13]. In this study, red LED was used. PPG technology is based on the use of light absorption to measure relative blood volume changes in the blood vessels. Thus, PPG is usually distorted by motion artefacts due to voluntary or involuntary movement by the subjects. A number of studies have attempted

to reduce the motion artefacts to enhance the signal-to-noise ratio [14-17]. As a result, a PPG waveform with minimized motion artefacts was successfully obtained, although all of the improvements were focused on the characteristics of the PPG waveform required for pulse oximetry. Therefore, the PPG signal is considered sufficiently accurate in obtaining the NNI required for HRV analysis. However, in this study, we have developed an optimal digital infinite impulse response (IIR) bandpass filter (IIR BPF) for accurate detection of NNI suitable for HRV analysis; the method is based on the transfer function of the analog second-order Butterworth bandpass filter. The developed IIR BPF can measure abnormal and normal heartbeat intervals accurately regardless of the variations in the amplitude of the PPG signal. It should be noted that an optimal digital IIR BPF based on a microcontroller will contribute to the development of precise HRV-based health monitoring services that uses the PPG signal.

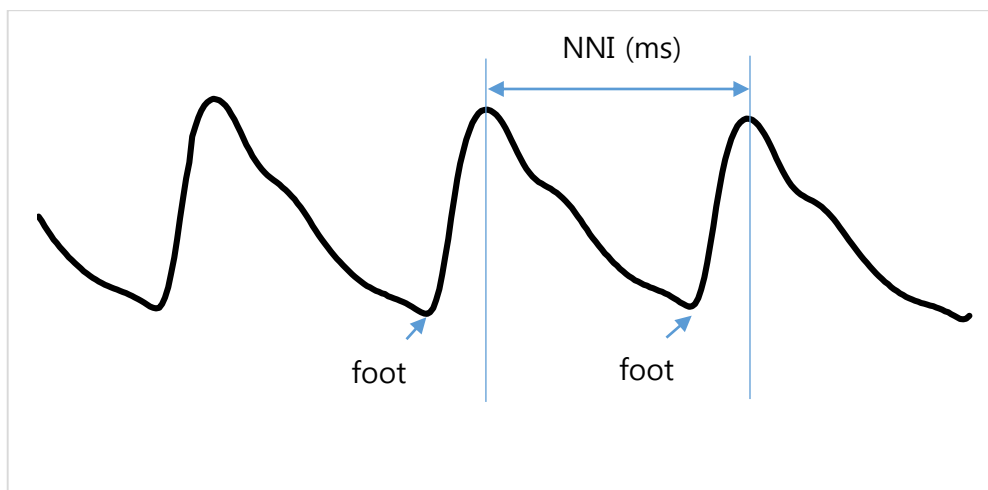


Figure 1. PPG signal representing the normal peak-to-peak interval in time series (NNI).

2. HRV PARAMETERS

Time-domain HRV parameters determine the number of variations in the time interval (in milliseconds) between successive heartbeats. Nonlinear HRV parameters quantify the structure and complexity of the NNI time series [18]. HRV is considered nonstationary and nonlinear. In general, HRV analysis consists of tens of parameters obtained from time-domain, frequency-domain, and nonlinear measurements. We have used three time-domain (SDNN, RMSSD, and SDSD) and two nonlinear (SD1 and SD2) HRV parameters to compare PPG with ECG as shown in Table 1. The parameters are calculated according to the following equations:

$$SDNN = \sqrt{\frac{\sum_{n=1}^{N-1} (NNI_n - \overline{NNI})^2}{N-1}} \quad (1)$$

$$RMSSD = \sqrt{\frac{1}{N-1} \sum_{n=1}^{N-1} [NNI_n - RR_{n-1}]^2} \quad (2)$$

$$SDSD = \sqrt{\frac{\sum (NNI_{diff} - \overline{NNI_{diff}})^2}{N-1}} \quad (3)$$

$$NNI_{diff} = NNI_n - NNI_{n-1}$$

Table 1. Descriptions of and comments for five HRV parameters

HRV parameters	Parameters	Description	Comment	Unit
Time domain	SDNN	Standard deviation of all interbeat normal-to-normal (NN) intervals	Long-term HRV	ms
	RMSSD	Root mean square of successive NN interval differences	Short-term HRV	ms
	SDSD	Standard deviation of differences between adjacent NN intervals	Short-term HRV	ms
Nonlinear domain	SD1	Standard deviation of the width of the Poincare plot	Short-term HRV	ms
	SD2	Standard deviation of the length of the Poincare plot	Long-term HRV	ms

Poincare plot analysis was performed according to the following equations (4-7). The HRV NNI data vector is defined as $x = (x_0, x_1, \dots, x_N)$. Two auxiliary vectors defined in (4) and (5), and all parameters of the Poincare plot are determined as follows:

$$x^a = (x_0, x_1, \dots, x_{N-1}) \quad (4)$$

$$x^b = (x_1, x_2, \dots, x_N) \quad (5)$$

$$x^c = \frac{x^a - x^b}{\sqrt{2}}, \quad x^d = \frac{x^a + x^b}{\sqrt{2}} \quad (6)$$

$$SD1 = \sqrt{\text{variance}(x^c)}, \quad SD2 = \sqrt{\text{variance}(x^d)} \quad (7)$$

The ellipse fitting method was used to calculate the dimensionless standard deviations (SD) of the distances of the points perpendicular to the axis of the line-of-identity ($y = -x$) and the SDs of the distances of the points along the axis of the line-of-identity ($y = x$), defined as SD1 and SD2, respectively, as shown in Figure 2. SD1 and SD2 indices represent the semi-minor (width) and semi-major (length) axes of the ellipse, respectively [19].

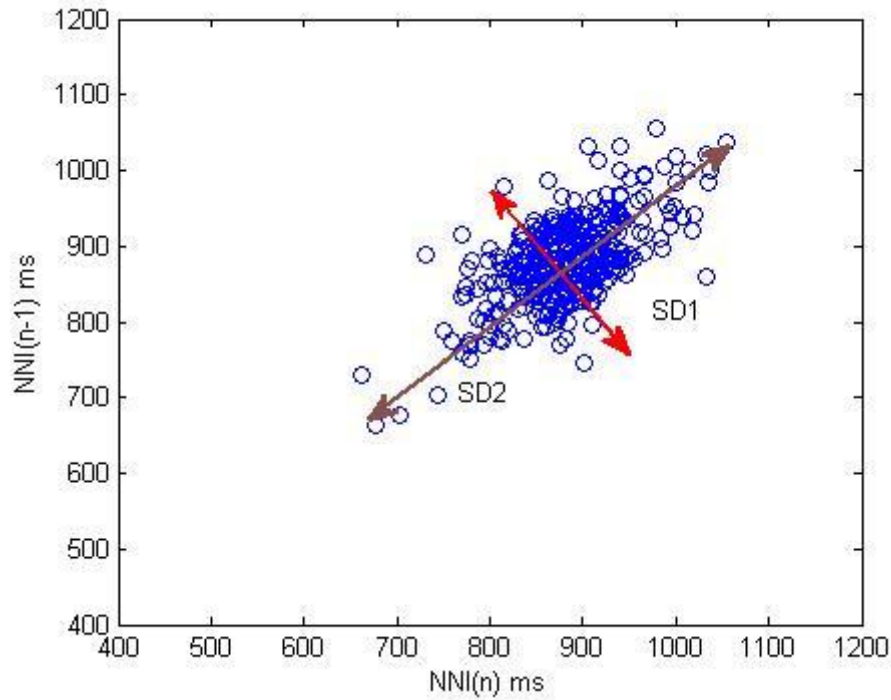


Figure 2. Poincare plot of 323 samples of NNI. The semi-major and semi-minor axes of the ellipse represent SD2 and SD1, respectively.

3. DIGITAL IIR BAND-PASS FILTER

A recursive IIR (Infinite Impulse Response) digital filter is an LTI (Linear Time Invariant) system based on the difference equation (8), which is called an IIR filter.

$$y[n] = -\sum_{k=1}^N a[k]y[n-k] + \sum_{k=0}^M b[k]x[n-k] \quad (8)$$

The transfer function is defined by the difference equation (9).

$$H(z) = \frac{b_0 + b_1z^{-1} + b_2z^{-2} + \dots + b_Mz^{-M}}{1 + a_1z^{-1} + a_2z^{-2} + \dots + a_Nz^{-N}} \quad (9)$$

$$H(z) = \frac{B(z)}{A(z)} \quad (10)$$

Where

$$B(z) = \sum_{n=0}^M b[n]z^{-n} \quad (11)$$

$$A(z) = 1 + \sum_{n=0}^N a[n]z^{-n} \quad (12)$$

H(z) can be written as

$$H(z) = \frac{z^{-M}}{z^{-N}} \cdot \frac{b_0z^M + b_1z^{M-1} + b_2z^{M-2} + \dots + b_M}{z^N + a_1z^{N-1} + a_2z^{N-2} + \dots + a_N} \quad (13)$$

The zeroes of $H(z)$ are the roots of the polynomial in equation (14).

$$b_0z^M + b_1z^{M-1} + b_2z^{M-2} + \dots + b_M \quad (14)$$

The poles of $H(z)$ are the roots of the polynomial in equation (15).

$$z^N + a_1z^{N-1} + a_2z^{N-2} + \dots + a_N \quad (15)$$

Our design of the IIR filter is based on analog prototype transfer function equivalent, the Butterworth filter, which maps the s-plane poles and zeros of the analog filter into the z-plane using the bilinear transformation. The bilinear z-transform is a mathematical transformation from the s-domain to the z-domain that preserves the frequency characteristics and is defined by equation (16).

$$s = \frac{2}{T} \frac{1-z^{-1}}{1+z^{-1}}, \quad \text{where } T = \text{sampling period} \quad (16)$$

Bilinear transformation gives a nonlinear relationship between the analog frequency ω_a and digital frequency ω_d . The frequency response of a digital filter is defined by setting $z = e^{j\omega_d T}$.

$$s = j\omega_a = \frac{2}{T} \frac{1-e^{-j\omega_d T}}{1+e^{-j\omega_d T}} = \frac{2}{T} \frac{e^{\frac{j\omega_d T}{2}} - e^{-\frac{j\omega_d T}{2}}}{e^{\frac{j\omega_d T}{2}} + e^{-\frac{j\omega_d T}{2}}} \quad (17)$$

$$\omega_a = \frac{2}{T} \tan \frac{\omega_d T}{2} \quad (18)$$

The cutoff frequencies of a digital filter must be tangentially warped compared with the cutoff frequencies of an analog filter used to design the digital filter. Therefore, it is necessary to prewarp the digital cutoff frequencies before designing the analog filter. Finally, an analog filter is designed with the appropriate warped cutoff frequencies. Applying the bilinear transformation to this analog filter gives a digital filter with the desired cutoff frequencies. Two cutoff frequencies are required to design a bandpass filter. We chose the first cutoff, and the second cutoff frequencies of 0.3 (f_{d1}) and 3 Hz (f_{d2}), respectively, for a sampling rate of 1 kHz ($T=10^{-3}$ sec). Application of the pre-warping transformation to equation (18) yields two analog cutoff frequencies.

$$\omega_{d1} = 2\pi \times 0.3 = 0.6\pi \text{ rad/sec} \quad (19)$$

$$\omega_{d2} = 2\pi \times 3.0 = 6.0\pi \text{ rad/sec} \quad (20)$$

$$\omega_{a1} = 0.03289868 \text{ rad/sec} \quad (21)$$

$$\omega_{a2} = 0.32898682 \text{ rad/sec} \quad (22)$$

4. IMPLEMENTATION

We applied the bilinear transformation that maps an imaginary axis of the s-plane onto a unit circle of the z-plane. Digital filter specifications, including the order of the filter and two cutoff frequencies, were converted to the specifications of an analog prototype Butterworth bandpass filter. Then, we determined the transfer function of the analog bandpass filter to transform the analog transfer function into the desired digital transfer function, $H(z)$ according to equation (23). All coefficients for the digital IIR BPF were calculated using MATLAB (2014b; MathWorks Inc., Natick, MA, USA), as shown in Table 2.

Table 2. IIR BPF coefficients calculated by MATLAB program

B[k]	Numerator	A[k]	Denominator
b0	0.000071094	a0	1.000000000
b1	0.000000000	a1	-3.975938926
b2	-0.000142189	a2	5.928172637
b3	0.000000000	a3	-3.928527652
b4	0.000071094	a4	0.976293942

Using the coefficients listed in Table 2, a digital IIR BPF transfer function was defined according to the following equation (23).

$$H(z) = \frac{0.000071094 + 0z^{-1} - 0.000142189z^{-2} + 0z^{-3} + 0.000071094z^{-4}}{1 - 3.975938926z^{-1} + 5.928172637z^{-2} - 3.928527652z^{-3} + 0.976293942z^{-4}} \quad (23)$$

Four poles and four zeros were calculated in the following values.

$$p_1 = 0.9893 + 0.0135i$$

$$p_2 = 0.9893 - 0.0135i$$

$$p_3 = 0.9987 + 0.0013i$$

$$p_4 = 0.9987 - 0.0013i$$

$$z_1 = -1.0019, z_2 = -0.9981, z_3 = 1.0019, z_4 = 0.9981 \quad (24)$$

The locations of the 4 poles and 4 zeros and the magnitude frequency response of the IIR BPF are shown in Figures 3 and 4, respectively.

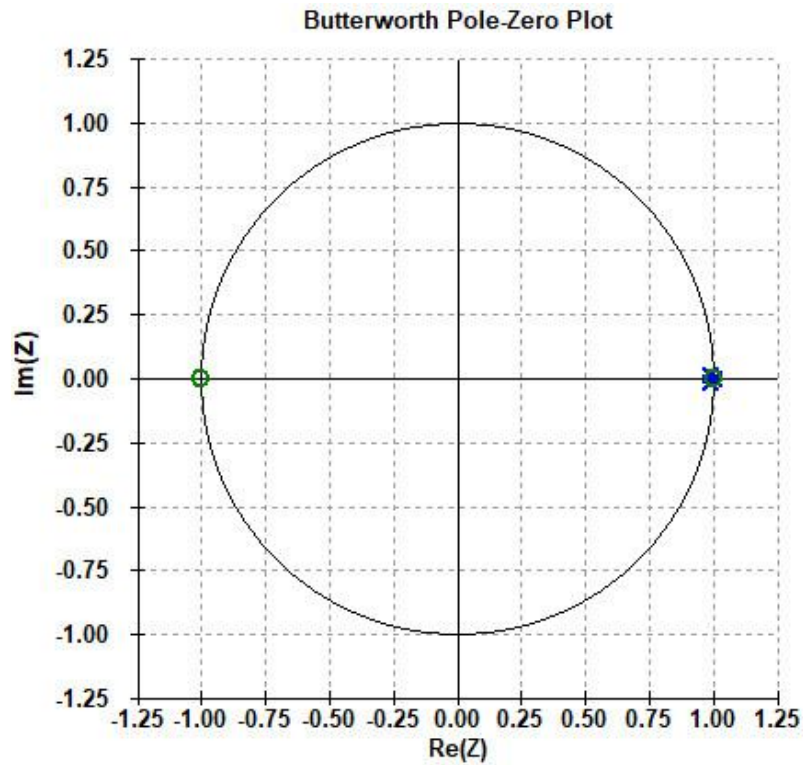


Figure 3. Locations of all poles and zeros on the z-plane for IIR BPF

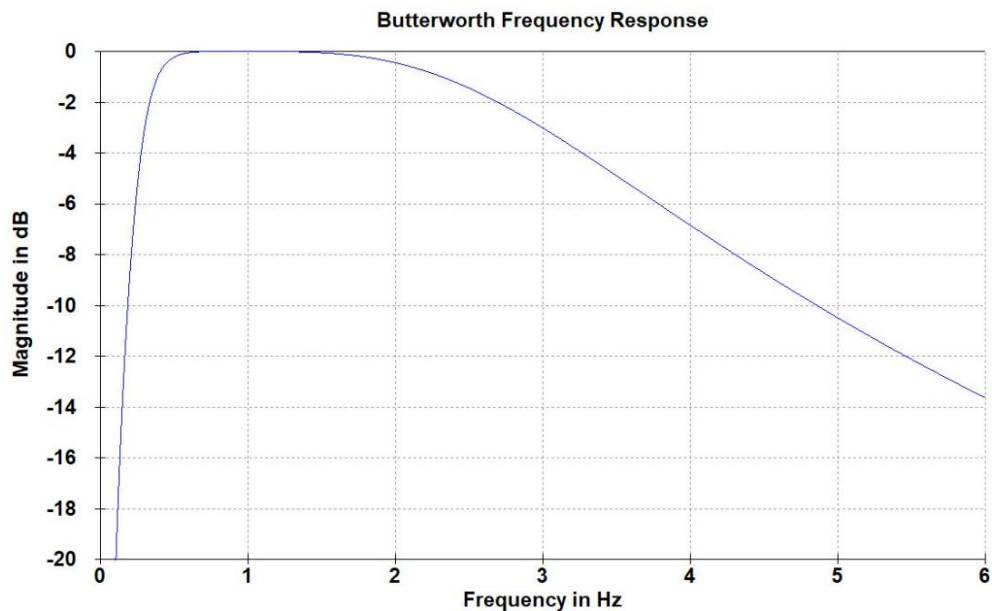


Figure 4. Magnitude frequency response of digital IIR BPF with -3 dB at the desired second cutoff frequency $f_{d2} = 3$ Hz.

The IIR BPF algorithm was programmed according to equation (25) based on a microcontroller (MSP430F6638, Texas Instruments, Dallas, TX, USA), embedded into a commercial pulse analyzer, TAS9VIEW (CANOPY9 RSA, IEMBIO. Ltd., Chuncheon-si, South Korea).

$$\begin{aligned} y[n] = & 0.00071094x[n] - 0.000142189x[n - 2] + 0.0000710941x[n - 4] \\ & + 3.975938926y[n - 1] - 5.928172637y[n - 2] + 3.928527652y[n - 3] \\ & - 0.976293942y[n - 44] \end{aligned} \quad (25)$$

5. DATA COLLECTION

The participant was in the sitting position in a quiet room and was not allowed to talk or move while the two measurements were performed. In this study, a 5-min HRV data pair of handgrip ECG recordings were obtained using a commercial HRV analyzer (CANOPY9 VIEW, IEMBIO. Ltd., Chuncheon-si, South Korea); the fingertip PPG recordings used in the IIR BPF testing were simultaneously obtained using a pulse analyzer equipment (TAS9VIEW or CANOPY9 RSA). The experimental setup was described in our previous study. The ECG and PPG signals were sampled at 1000 samples s^{-1} . Two recordings were inspected to select the data pairs that did not have any time delay that could influence the results [20].

6. RESULTS

The results of digital IIR BPF with and without a motion artefact introduced in the PPG signal are presented in Figure 5. Upper and lower waves represent the PPG and digital IIR BPF output acquired using a microcontroller, respectively. Figure 5(b) illustrates the comparison between PPGs with and without a motion artefact. The results indicate that the developed IIR BPF can efficiently remove the motion artefact from the noisy PPG signal. Waveform of the IIR BPF output from the artefact-free PPG was slightly different from that of the PPG with an artefact; however, an accurate heartbeat interval could be obtained through an analog comparator to create a pulse back into a microcontroller. Motion artefacts were introduced by vertical or horizontal movements of the finger during measurement. The calculation of NNI (ms) depends on the peak-to-peak values of the PPG signal. Thus, it is important that the optimal IIR BPF algorithm preserves this characteristic in the filtered output, as indicated by the lower wave in Figure 5(b). Because the PPG signal is produced within the range from 0.5 to 4.0 Hz [14], we determined two cutoff frequencies of the bandpass filter, 0.3 and 3.0 Hz. The original PPG signal was initially processed by an analog RC filter to filter out

the high frequency noise and then, the signal was input into an ADC (analog-to-digital converter) pin port on a microcontroller.

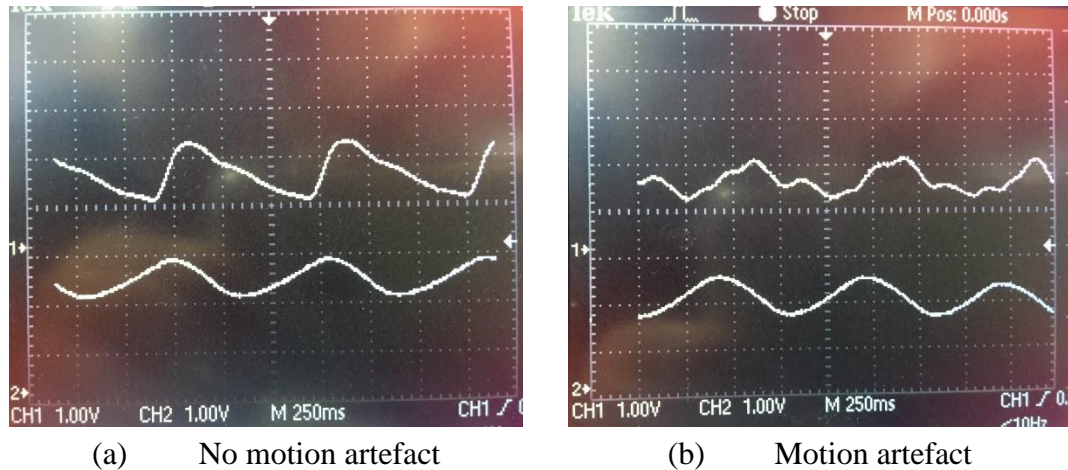


Figure 5. An IIR BPF output (lower wave) for the detection of NNI based on the PPG signal (upper wave) and the impact of a motion artefact.

The HRV parameters derived from PPG and ECG were compared based on the relative errors as shown in Table 3. The smallest errors are observed in the case of SDNN in the 2nd test and in the case of SDD in the 1st test with relative errors of 0.00 and 0.66, respectively. The highest errors were observed in the case of SD1 with relative errors of 0.68 % and 2.40 % for the 1st and 2nd test, respectively. All parameters derived from the HRV datasets obtained by two different methods (PPG and ECG recordings) were within 2.4 % relative error margin. The smallest difference between PPG and ECG among the five HRV parameters is SD2 (relative error of 0.86 % and 0.53 %, respectively). Therefore, the results show that there were no significant differences between the PPG and ECG datasets.

Table 3. Values of five HRV parameters for two 5-min recordings of the PPG-ECG data pairs.

Measurement	Type	SDNN	RMSSD	SDSD	SD1	SD2
1 st test	PPG1	57.87	49.75	49.68	35.23	73.65
	ECG1	57.47	50.09	50.01	35.47	73.02
	Relative Error (%)	0.69	-0.68	0.66	0.68	0.86
2 nd test	PPG2	57.71	49.44	49.37	35.01	73.82
	ECG2	57.71	50.62	50.54	35.85	73.43
	Relative Error (%)	0.00	-2.38	2.37	2.40	0.53

7. CONCLUSIONS

Recursive IIR BPF allowed us to achieve the desired characteristics of the frequency response using a filter of lower order than that in the case of a nonrecursive filter. The recursive filter developed in the present work has all poles and zeros in close proximity to the unit circle on the z-plane. We used the bilinear transformation method to convert a Laplace transfer function of an analog prototype Butterworth filter into a digital transfer function. However, all poles of the IIR coefficients were be very close to the unit circle. Thus, IIR BPF performance is very sensitive to changes in the values of the poles, resulting in a high possibility that the response of the actual digital IIR filter can deviate from the desired response. For a filter circuit to be stable, all its poles must lie within the unit circle on the z-plane. Therefore, to ensure the stability of the IIR filter, the poles must be specified with high accuracy (9 decimal places) due to the implementation of a 16-bit microcontroller. The positions of the poles in the z-plane are the important factors in determining the stability of the IIR BPF system. It may be impossible or very expensive to implement IIR BPF with the desired specification as an analog filter design with an RLC circuit because of the required tolerances in the component values and in the electrical characteristics of the operational amplifier. The frequency response of the Butterworth filter, a maximally flat filter, has no ripples in the passband or the stopband. A smooth, monotonically decreasing frequency response in the transition region is an advantage of the Butterworth filter. However, the frequency response of the Chebyshev filter has a narrower transition range than that of the Butterworth filter, resulting in a passband or stopband with more ripples. Therefore, the

Butterworth prototype filter is more suitable than the Chebyshev filter because PPG has oscillations in the amplitude due to an optical measurement that senses the blood volume changes. We recommend that the IIR BPF developed in the present study is implemented into a PPG system for the detection of NNI in HRV analysis as a replacement for the ECG system.

ACKNOWLEDGEMENTS

This work was supported by the Hallym University Research Fund (HRF-201811-012).

REFERENCES

- [1] Task Force of the European Society of Cardiology the North American Society of Pacing Electrophysiology. Heart Rate Variability: standards of measurement, physiological interpretation, and clinical use. *Circulation*, 93, 1043-1065 (1996).
- [2] Karemaker, J.M. An introduction into autonomic nervous function. *Physiological Measurement*, 38(5), R89-R118 (2017).
- [3] Karemaker, J.M. How the vagus nerve produces beat-to-beat heart rate variability; experiments in rabbits to mimic in vivo vagal patterns. *Journal of Clinical and Translational Research*, 1(3), 190-204 (2015).
- [4] Malliani, A. Cardiovascular neural regulation explored in the frequency domain. *Circulation*, 84, 482-492 (1991).
- [5] Pomeranz, B., Macaulay, R.J., Caudill, M.A., Kutz, I., Adam, D., Gordon, D., Kilborn, K.M., Barger, A.C., Shannon, D.C., Cohen, R.J. Assessment of autonomic function in humans by heart rate spectral analysis. *The American Journal of Physiology*, 248(1), H151-H151 (1985).
- [6] Peng, R.C., Zhou, X.L., Lin, W.H., Zhang, Y.T. Extraction of heart rate variability from smartphone photoplethysmograms. *Computational and Mathematical Methods in Medicine*, 2015(1), 1-11 (2015).
- [7] Lu, S., Zhao, K., Ju, K., Shin, K., Lee, M., Shelley, K., Chon, K.H. Can photoplethysmography variability serve as an alternative approach to obtain heart rate variability information? *Journal of Clinical Monitoring and Computing*, 22(1), 23-29 (2008).
- [8] Gil, E., Orini, M., Bailon, R., Vergara, J.M., Mainardi, L., Laguna, P. Photoplethysmography pulse rate variability as a surrogate measurement of heart rate variability during non-stationary conditions. *Physiological Measurement*, 31(9),

1271-1290 (2010).

- [9] Charlot, K., Cornolo, J., Brugniaux, J.V., Richalet, J.P., Pichon, A. Interchangeability between heart rate and photoplethysmography variabilities during sympathetic stimulations. *Physiological Measurement*, 30(12), 1357-1369 (2009).
- [10] Tamura, T., Maeda, Y., Sekine, M., Yoshida, M. Wearable photoplethysmographic sensors-past and present. *Electronics*, 3, 282-302 (2014).
- [11] Roggan, A., Friebel, M., Do Rschel, K., Hahn, A., and Mueller, G. Optical properties of circulating human blood in the wavelength range 400-2500 nm. *Journal of Biomedical Optics*, 4(1), 36-46 (1999)
- [12] Cui, W., Ostrander, L.E., Lee, B.Y. In vivo reflectance of blood and tissue as a function of light wavelength. *IEEE Transaction on Biomedical Engineering*, 37, 632-639 (1990).
- [13] Meada, Y., Sekine, M., Tamura, T. The advantage of green reflected photoplethysmograph. *Journal of Medical Systems*, 35, 829-834 (2011).
- [14] Ram, M.R., Madhav, V.M., Krishna, E.H., Komalla, N.R., Reddy, K.A. A novel approach for motion artifact reduction in PPG signals based on AS-LMS adaptive filter. *IEEE Transaction on Instrumentation and Measurement*, 61(5), 1445- 1457 (2012).
- [15] Rusch, T.L., Sankar, R., Scharf, J.E. Signal processing methods for pulse oximetry. *Computers in Biology and Medicine*, 26(2), 143-159 (1996).
- [16] Barreto, A.B., Vicente, L.M., Persad, I.K. Adaptive cancellation of motion artifact in photoplethysmographic blood volume pulse measurements for exercise evaluation. In *Proceedings IEEE-EMBC/CMBEC*, 2, 983-984 (1995).
- [17] Krishnan R., Natarajan, B., Warren, S. Two-stage approach for detection and reduction of motion artifacts in photoplethysmographic data. *IEEE Transactions on Biomedical Engineering*, 5(8), 1867-1876 (2010).
- [18] German-Sallo, Z., German-Sallo, M. Non-linear methods in HRV analysis. *Procedia Technology*, 22, 645-651, (2016).
- [19] Brennan, M., Palaniswami, M., and Kamen, P. Do existing measures of Poincare plot geometry reflect nonlinear features of heart rate variability. *IEEE Transactions on Biomedical Engineering*, 48, 1342-1347 (2001).
- [20] Ahn, J.M. Heart rate variability (HRV) analysis using simultaneous handgrip electrocardiogram and fingertip photoplethysmogram. *Advances in Information Sciences and Service Sciences (AISS)*, 5(13), 164-170 (2013).

2022

Jeom Keun Kim, Jae Mok Ahn